Accurate experimental and theoretical comparisons between superconductor-insulator-superconductor mixers showing weak and strong quantum effects

W. R. McGrath [a] and P. L. Richards
Department of Physics, University of California, Berkeley, California 94720

D. W. Face [b] and D. E. Prober
Section of Applied Physics, Yale University, P. O. Box 2157, New Haven, Connecticut 06520

F. L. Lloyd
National Bureau of Standards, Boulder, Colorado 80303

(Received 10 August 1987; accepted for publication 17 November 1987)

We have made a systematic study of the gain and noise in superconductor-insulator-superconductor mixers employing Ta based, Nb based, and Pb-alloy based tunnel junctions. These junctions displayed both weak and strong quantum effects at a signal frequency of 33 GHz. The effects of energy gap sharpness and subgap current were investigated and are quantitatively related to mixer performance. Detailed comparisons are made of the mixing results with the predictions of a three-port model approximation to the Tucker theory. We have measured mixer performance with a novel test apparatus which is accurate enough to allow for the first quantitative tests of theoretical noise predictions. We find that the three-port model of the Tucker theory underestimates the mixer noise temperature by a factor of about 2 for all of our mixers. In addition, predicted values of available mixer gain are in reasonable agreement with experiment when quantum effects are weak. However, as quantum effects become strong, the predicted available gain diverges to infinity, which is in sharp contrast to the experimental results. Predictions of coupled gain do not always show such divergences.

I. INTRODUCTION

The nonlinear quasiparticle tunneling characteristics of superconductor-insulator-superconductor (SIS) tunnel junctions are well adapted for low-noise heterodyne mixing. The discovery of these properties has led to the rapid development of SIS mixers for use in low-noise millimeter wave receivers for radio astronomy. Their performance has surpassed that of other technologies in recent years.[1–6] The quantum theory of mixing, worked out by Tucker,[7] predicts strong quantum effects when these devices are operated at millimeter wave frequencies. The available gain of a mixer, G_A, which is the ratio of the available IF (intermediate frequency) output power to the available rf (radio frequency) input power, is predicted to exceed unity (0 dB). Classical mixer theory, on the other hand, predicts $G_A < 0$ dB. The mixer noise temperature, T_M, can approach a fundamental lower limit, $T_Q = \hbar\omega/k$ (Refs. 8–10) set by the Heisenberg uncertainty principle. In order to realize these predictions, tunnel junctions must meet two important requirements. First, the conductance below the superconducting energy gap voltage V_G must be small. Second, the voltage width ΔV_G of the current rise at V_G must be less than $\hbar\omega/e$ for the frequency of interest. In addition, it is necessary to provide the proper rf source impedances. Also, the proper IF load impedance is required before coupled gain is observed.

Sn junctions[1] and Ta/PbBi junctions,[6] which meet these criteria, have been used to observe strong quantum effects at 36 GHz. These effects have also been observed in Pb-alloy junctions,[3,11] which satisfy the above criteria for frequencies near 90 GHz. However, most of the research[5] on SIS mixers has not shown large gain, either because the junctions used did not meet the requirements stated, or because the required rf impedance was not supplied. Another problem arises from the fact that the mixer is usually tuned for maximum coupled gain, so regions of large available gain can be missed. This important point is discussed in more detail in Sec. III.

In order to achieve all the proper conditions to fully optimize the gain and noise of an SIS mixer, a detailed understanding of the Tucker theory is needed. This requires accurate measurements of mixer performance for checking the predictions of the theory. In order to make accurate tests, we have employed a novel apparatus[12] using low-temperature loads (blackbodies) which allow mixer noise temperature to be measured with an accuracy of better than ± 1 K and mixer gain with an accuracy of $\pm 8\%$. This represents a substantial improvement over the accuracy of previously reported noise measurements.[1–3] Quantitative studies of mixer gain have been carried out by several groups[5] but similar studies of mixer noise have been hampered by a lack of accurate measurements. The work reported here represents the first systematic study of noise in SIS mixers with an accuracy high enough to quantitatively test the shot-noise predictions of the Tucker theory. High accuracy is particularly impor-

[a] New address: Jet Propulsion Laboratory, 4800 Oak Grove Dr., Pasadena, CA 91109.
[b] New address: Department of Physics, Rm. 13-2145, M.I.T., Cambridge, MA 02139.

tant for several of our mixers for which the mixer noise temperature approaches the quantum limit $T_Q = 1.7$ K at 33 GHz.

In order to explore the effect of variations in I-V curve quality on mixer performance, we have made a systematic study of gain and noise in SIS mixers at 33 GHz employing Ta and Nb based junctions, as well as Pb-alloy junctions.[13] The sharp I-V curves of the Ta based junctions had a $\Delta V_G \ll \hbar\omega/e$ and very low subgap currents. These junctions showed large available gain, $G_A > 0$ dB, and a noise temperature within a factor of 2 of the quantum limit, $T_M < 2T_Q$. The I-V curve of the Nb junction was sharp at a low liquid-helium (LHe) bath temperature, $T_b = 1.3$ K but rounded at higher temperature, $T_b = 4.2$ K. This allowed the same junction to show strong and weak quantum effects by simply changing the bath temperature. The advantage of using the same junction is that the contribution to the rf embedding impedances which depend on the junction geometry and capacitance remain unchanged. Since mixer performance is strongly dependent on the embedding impedances, keeping these constants isolates the effects of changing the I-V curve quality. This mixer showed a factor of 2 increase in gain and a similar decrease in noise temperature when cooled from 4.2 to 1.3 K. Finally, the Pb-alloy junction, which had a rounded I-V curve such that $\Delta V_G > \hbar\omega/e$, showed only weak quantum effects with $G_A < 0$ dB. However, the mixer noise temperature was reasonably low, less than 8 K.

We have made detailed comparisons of our mixing results with the predictions of a three-port model of the Tucker theory and found good agreement with the measured gain for a Pb-alloy junction. This is consistent with other reported studies which found good agreement between theory and experiment when quantum effects were weak (see Ref. 5 for a review). The use of Nb and Ta junctions with sharp I-V curves and the use of our accurate measurement apparatus, however, gives a more critical test of the Tucker theory when quantum effects are strong. In general, the theoretical predictions of the three-port model strongly diverge from the measured values in this regime. Infinite available mixer gain is predicted and the range of embedding impedances, for which this infinity exists, increases for bias voltages near the energy gap. The theory also consistently underestimates the mixer noise temperature by about a factor of 2 for all junctions tested, regardless of whether quantum effects were strong or weak. One possible explanation for these discrepancies is the harmonic response of the mixer which is not included in the calculations. This effect may become more important as quantum effects become stronger.

The sections of this paper are arranged as follows. Section II outlines the fabrication techniques and parameters of the junctions tested as mixers at 33 GHz. The definition of mixer gain and noise temperature we used and the quantum limits on the noise are discussed in Sec. III. The measurement techniques used to evaluate mixer performance are summarized in Sec. IV. The results of the mixing experiments are presented and discussed in Sec. V. Section VI describes the calculations using a three-port model of the Tucker theory.

II. JUNCTION FABRICATION

The tantalum junctions were fabricated with a novel step-defined technique developed by Face and coworkers[6,14] using a 280-nm-thick Ta base electrode on a Si substrate, dc plasma oxidation, and a 300-nm-thick PbBi counterelectrode. The Ta junction Ta-1 listed in Table 1 is the only exception in that a pure Pb counterelectrode was used rather than PbBi. The junction geometry was defined by a 0.7-μm high by 2-μm-wide step etched in the substrate. The electrodes were deposited at 45° to the normal, producing the junction overlap area of $\sim 2\,\mu m^2$. The niobium junctions were fabricated by a similar process using a 250-nm-thick Nb base electrode.

The Pb-alloy junctions were fabricated at NBS Boulder using a 200-nm-thick PbInAu base electrode on a Si substrate, rf plasma oxidation, and a 400-nm-thick PbBi counterelectrode. The junction area of 16 μm^2 was defined by a window in a 300-nm-thick SiO layer located between the two electrodes.

The properties of several different junctions tested as SIS mixers are listed in Table I. The normal state resistance of the junction is R_N. The critical current density was determined from the relation $J_c = I_c/$ area where the critical current I_c was obtained using the relation $I_c = (0.7)V_G/R_N$.[15] The sum gap voltage, V_G, is defined to be the voltage corre-

TABLE I. dc electrical properties of the SIS tunnel junctions tested as mixers at 33 GHz. The junction properties were measured at the LHe bath temperature listed under T_b. The normal-state resistance of the junction is R_N, J_c is the critical current density, ΔV_G is the voltage width of the current rise at the sum gap, I_{SG} is the subgap current measured at 80% of the sum gap voltage and is expressed as a percentage of the critical current, and $\omega_S R_N C_J$ is the normalized junction relaxation time parameter. All of the Ta and Nb based junctions had a $Pb_{0.9}Bi_{0.1}$ counterelectrode except for junction Ta-1 which had a pure Pb counterelectrode.

Junction	T_b (K)	R_N (Ω)	J_c (A/cm^2)	ΔV_G (μV)	I_{SG} (%)	$\omega_S R_N C_J$
Ta-1	1.3	101	660	83	0.7	6.0
Ta-2	1.3	44	1600	20	0.9	2.7
	2.0	44	1600	31	2.0	2.7
Ta-3	1.3	70	1080	22	1.0	4.3
Ta-4	1.3	26	2900	35	1.0	1.5
Nb	1.3	72	1430	35	4.0	4.2
	4.2	72	1370	250	7.7	4.2
Pb-alloy	1.3	45	300	330	4.5	5.8

sponding to the inflection point of the current rise and is given approximately by the relation $V_G \sim (\Delta_1 + \Delta_2)/e$, where Δ_1 and Δ_2 are the energy gaps of the two superconductors. The voltage width ΔV_G of the current rise at the sum gap is given by the difference between the voltages for the current to rise from 10% to 90% of I_c. The subgap current, I_{SG}, was measured at 80% of V_G and is given as a percentage of I_c. The normalized junction relaxation time parameter $\omega_s R_N C_J$ is the product of the angular signal frequency ω_s, the junction capacitance C_J, and the junction normal-state resistance R_N. A value of C_J for the Pb junction was determined from data published by Magerlein[16] relating capacitance per unit area C/A to J_c. This method gives $C_J = 620$ fF (femtofarads). The capacitance for the Nb and Ta junctions was estimated using the value given in the literature[17] for Nb junctions of 140 fF/μm^2, which gives $C_J = 280$ fF.

All of the Ta and Nb junctions discussed in this paper displayed a gradual increase in R_N when exposed to air at room temperature. Junction Ta-3 with $R_N = 70\,\Omega$ in Table I was obtained from the 44 Ω junction Ta-2 by exposure to air for several hours. This change in junction properties with time has subsequently been eliminated by the use of an In overlayer on the PbBi counterelectrode.[14,18]

III. MIXER GAIN AND NOISE

A. Definition of available and coupled gain

In discussing mixer performance it is necessary to define both an available mixer gain and a coupled mixer gain. The available mixer gain G_A is defined as the ratio of available power from the mixer at the intermediate frequency (IF), $P_A^{\rm IF}$, to the available power at the signal frequency $P_A^{\rm rf}$,

$$G_A = P_A^{\rm IF}/P_A^{\rm rf}. \tag{1}$$

The term "available power" refers to the power that would be coupled into a matched load (the reflected power is zero under these conditions). Thus, G_A is independent of the IF load impedance Z_L. In most practical experimental arrangements, Z_L is not matched to the IF output impedance $Z_{\rm IF}$ of the mixer, and thus not all of the available IF power is coupled out (some power is reflected back into the mixer). In this case, the coupled gain G_c of the mixer is defined as the ratio of power coupled out of the mixer at the IF to the available signal power and can be written as follows:

$$G_c = G_A(1-|\rho|^2), \tag{2}$$

where $|\rho|^2$ is the power reflection coefficient at the IF output of the mixer. This coefficient is related to the mixer IF impedance and load impedance by the relation

$$1 - |\rho|^2 = [4\mathrm{Re}(Z_L)\mathrm{Re}(Z_{\rm IF})/|Z_L + Z_{\rm IF}|^2]. \tag{3}$$

Tucker has shown[7] that as $\mathrm{Re}(Z_{\rm IF})$ approaches infinity (and even becomes negative), that G_A becomes infinite.[19] In our mixer experiments, we maximized G_c as this is the most straightforward procedure (see Sec. IV) and then measured the power reflection coefficient $|\rho|^2$ to calculate G_A from Eq. (2). However, since $|\rho|^2$ can approach unity as G_A becomes large, it is possible to miss the tuning conditions that produce large available gain. Thus, it is desirable to minimize the IF impedance mismatch. The dramatic effect of a proper impedance match on coupled gain has recently been demonstrated in a high gain mixer by Räisänen *et al.*[11]

B. Definition of noise temperature

For several reasons it is convenient to characterize the noise of a mixer by giving the noise power per unit bandwidth P_N/B, at the rf input.[20,21] This quantity can be directly measured using hot/cold load techniques.[12,20] The total input noise power for a heterodyne receiver can be found by directly adding the noise power per unit bandwidth for each component referred to the rf (receiver) input. Also, this quantity can be easily compared with the shot-noise predictions of the Tucker theory.[7]

The noise power per unit bandwidth of a mixer is often expressed as an effective temperature. This noise temperature T_M is defined by the relation

$$P_N/B = k_B T_M, \tag{4}$$

where k_B is Boltzmann's constant. We use this definition of T_M in this paper. Although there appears to be no uniform standard, Eq. (4) is commonly used by other authors.[5] In our previous publications[1,6,12] we used the true thermodynamic temperature T_T to characterize the noise. This was done by equating P_N/B to the power radiated by a blackbody at the rf frequency using the Planck law:

$$P_N/B = \hbar\omega/[\exp(\hbar\omega/k_B T_T) - 1], \tag{5}$$

where $\hbar$ is Planck's constant divided by 2π and ω is the angular rf frequency. Since in our previous publications T_M was defined with Eq. (5) an appropriate conversion must be made for our previous results. In the limit of $k_B T_M \gg \hbar\omega$, Eq. (5), reduces to Eq. (4). Unfortunately, when the noise temperature is defined with Eq. (5), the temperature is not linearly related to the noise power, and noise temperatures are not additive.

C. Noise in the quantum limit

The quantum limit for noise in SIS mixers has recently been discussed by a number of authors[5,8–10,22,23] and is briefly summarized here. The general theoretical treatment by Caves[8] shows that any narrow bandwidth linear amplifier which is phase preserving (Caves refers to this as a "phase insensitive" amplifier) must add a noise power referred to the input of

$$P_N \geqslant |1 - 1/G_P|\hbar\omega B/2, \tag{6}$$

where G_P is the photon number gain. A SIS junction is a nonlinear device for large drive such as the local oscillator, but its small signal properties satisfy Caves' conditions for a linear amplifier since the IF output power is proportional to the rf input power and the phase information is preserved. Also, an SIS mixer almost always operates with a large photon number gain, $G_P \gg 1$, and thus the minimum noise power given by Eq. (6) is

$$P_N = \hbar\omega B/2. \tag{7}$$

This minimum noise is a direct consequence of the Heisenberg uncertainty principle.

The Tucker theory[7] predicts the shot-noise power in an SIS mixer due to the quasiparticle tunneling currents driven by the local oscillator (LO). This shot-noise power can approach zero for a double-sideband (DSB) mixer and $\hbar\omega B/2$ for a single-sideband (SSB) mixer.[9,10] In the case of the DSB

mixer, a zero-point fluctuation noise ($\hbar\omega B/2$) arises from the image termination[9] and thus preserves Caves' general prediction, Eq. (7).

Evidence for the coupling of zero-point fluctuations from the dissipative parts of the rf terminations to tunnel junctions has been reported in tunnel junction SQUIDS.[24] Zorin[23] suggests that the zero-point fluctuations in the terminating conductance G_i at the image frequency, ω_i, port of an SIS mixer can be included by using a current generator of mean-square amplitude

$$\langle i^2\rangle = 2G_i\hbar\omega B\coth(\hbar\omega_i/2k_BT). \tag{8}$$

Devyatov *et al.*[22] and Zorin[23] also argue that this lumped circuit approach is equivalent to a complete quantum-mechanical treatment including zero-point fluctuations. Recent work by Wengler and Woody[10] has shown that these results are rigorously correct when all the classical currents and voltages in the Tucker theory are quantized. That work[10] also shows that the minimum noise added by an SIS mixer is $\hbar\omega B/2$ for an arbitrary image termination.

By including the zero-point fluctuations in the signal termination ($\hbar\omega B/2$), we obtain the total minimum noise power at the rf input of the mixer,

$$P_N = \hbar\omega B. \tag{9}$$

Expressed as a temperature using Eq. (4) we obtain,

$$T_Q = \hbar\omega/k_B. \tag{10}$$

For a frequency of $\omega/2\pi = 36$ GHz, Eq. (10) gives $T_Q = 1.7$ K. This is the appropriate limit for comparison with our experimental results because our measurement technique (see Sec. IV) yields the total noise power at the rf input to the mixer including zero-point fluctuations in the signal port.

IV. MEASUREMENT TECHNIQUES

Accurate measurements of mixer gain and noise are required to properly evaluate each type of tunnel junction. The method we used, employing cryogenically cooled variable-temperature loads, is described elsewhere[12] and is briefly discussed here. The mixer block was a full height Ka band (26.5–40.0 GHz) waveguide with an adjustable noncontacting backshort and a screw tuner located $3\lambda_g/4$ in front of the junction. Scale model measurements[25] showed that these tuning elements can provide a very wide range of rf source impedances to the junction in a bandwidth of $\sim$100 MHz. The power at the LO frequency of 34.5 GHz was fed to the mixer through a cooled $\sim$30 dB crossed-guide coupler which also served to reduce room-temperature thermal noise. The straight-through arm of the coupler was terminated by a specially designed variable-temperature rf waveguide load[12] which provided a calibrated signal power P_1.

The mixer was tuned by injecting a monochromatic signal at either 33 GHz (lower sideband) or 36 GHz (upper sideband) in through the LO waveguide. In each experiment, the junction dc bias voltage V_0, the LO power level, the position of the backshort, and the position of the screw tuner were adjusted iteratively to maximize coupled gain G_c. This procedure maximized the output power P_{IF} of the 1.5-GHz IF system which was easily monitored with a direct detector. The ratio of G_c in the optimized sideband to G_c in the other sideband is termed "sideband ratio" and will be referred to in later sections.

The IF power from the mixer was coupled to a cooled GaAs field-effect-transistor (FET) amplifier,[26] through a quarter-wave microstrip matching transformer. A 30-dB bidirectional coupler was used to measure the reflection coefficient $|\rho|^2$ for the IF power, which was less than 0.1 for most junctions and experimental conditions. A cooled coaxial switch was used to compare the IF power P_0 from the matching transformer with the calibrated power P_2 from a specially designed variable-temperature IF coaxial load.[12]

In each measurement, five values of rf load temperature T_1 between 1.5 and 20 K were chosen, yielding five values of P_1. For each P_1, the IF load temperature T_2 was adjusted until P_2 equaled the IF output power of the mixer P_0. Under these conditions, the relationship between P_1 and P_2 is

$$P_1 = P_2/G_c - P_M. \tag{11}$$

Here G_c is the coupled gain of the mixer and P_M is the mixer noise power referred to the rf input of the mixer block. The powers P_1 and P_2 were calculated from the physical temperatures of the loads, T_1 and T_2, respectively, using the Planck law given in Eq. (5). In practice, G_c and P_M/B are obtained by plotting P_1/B vs P_2/B for several pairs of data points. Notice that the IF bandwidth B need not actually be measured.

By carefully calibrating our components and applying several small corrections for losses and reflections,[12] we could measure the coupled mixer gain G_c into our 50-Ω IF system to an accuracy of $\pm$ 8%. The available gain G_A was calculated using Eq. (2) to an accuracy of about $\pm$ 10%. The mixer noise temperature T_M was measured to better than $\pm$ 1 K.

By plotting the rf power per unit bandwidth, P_1/B, versus the IF system output power we obtained the overall receiver noise power per unit bandwidth, P_R/B and receiver noise temperature ($T_R = P_R/k_BB$) for our measurement system referred to the 1.5-K rf input. T_R includes all of the system losses, impedance mismatches, and the IF system noise temperature, $T_{IF} \sim 15$ K. In some experiments where a complete set of values of P_{IF} was not recorded, the receiver noise was calculated using the measured values of T_M, T_{IF}, and G_c using the relationship

$$T_R = T_M + T_{IF}/G_c. \tag{10}$$

In order to explore the double-sideband performance of some of our mixers, lower IFs of 25, 100, and 300 MHz were used. As discussed below in Sec. V, it is expected that higher mixer gain should be observed for a DSB mixer. For these measurements, the first stage of the IF system was a commercially available wideband, 1–500 MHz, room-temperature amplifier. No IF matching transformer was used at low IFs. Mixer gain was measured by injecting a monochromatic signal at a frequency near 36 GHz in through the crossed-guide coupler. Corrections were made for the combined $\sim$22.5 dB loss of the stainless-steel waveguide and crossed-guide coupler and for the $\sim$0.25 dB loss in the cooled stainless-steel coaxial IF transmission line. The output impedance of the mixer, Z_{IF}, was estimated from the dynamic

TABLE II. Summary of mixer results with a 1.5-GHz IF, and theoretical calculations using a three-port model of the Tucker theory. The junctions are numbered the same as in Table I. Photon step $n = 3$–4 refers to a dc bias voltage about midway between steps 3 and 4 (similarly for $n = 7$–8). G_A is the available mixer gain, T_M is the mixer noise temperature, and T_R is the receiver noise temperature. The symbol ** means not measured or calculated.

Junction	T_b (K)	Photon step n	Expt. G_A (dB)	Theory G_A (dB)	Expt. T_M (K)	Theory T_M (K)	Expt. T_R (K)
Ta-1	1.3	1	-4.7 ± 0.4	**	3.0 ± 1	**	47 ± 2
Ta-2	1.3	1	-4.0 ± 0.2	∞	5.3 ± 0.4	2.5	52 ± 2
	1.3	2	-2.4 ± 0.2	∞	4.9 ± 0.4	2.5	38 ± 2
	1.3	4	0.41 ± 0.4	∞	4.4 ± 0.4	2.3	30 ± 1
	2.0	4	0.41 ± 0.4	∞	4.8 ± 0.5	2.7	29 ± 1
	1.3	4[a]	-0.81 ± 0.3	∞	3.9 ± 0.4	2.3	24 ± 1
	1.3	3–4	-12 ± 0.5	-11	6.8 ± 3.4	2.7	**
Nb	1.3	4	-2.5 ± 0.2	∞	4.7 ± 0.8	3.2	42 ± 2
	4.2	4	-5.7 ± 0.3	-3.9	8.2 ± 1.6	4.5	96 ± 2
Pb-alloy	1.3	4	-5.5 ± 0.3	-5.2	7.5 ± 0.8	4.0	58 ± 3
	1.3	6	-5.1 ± 0.3	-4.6	6.4 ± 0.5	3.3	50 ± 3
	1.3	7–8	-5.5 ± 0.3	-4.6	5.7 ± 0.6	3.4	55 ± 4
	1.3	8	-4.3 ± 0.2	-4.5	5.6 ± 0.5	3.4	43 ± 3

[a] These tuning conditions gave the lowest receiver noise temperature.

resistance R_d ($R_d = dV_0/dI_0$) of the pumped dc I-V curve at a fixed dc bias voltage. The reflection coefficient $|\rho|^2$ was then calculated using Eq. (3) and an IF load impedance Z_L of 50 Ω. These values of $|\rho|^2$ estimated from the dc dynamic resistance agreed to within about 10% with the values derived from power reflection measurements made with a directional coupler at 25 MHz. However, the Tucker theory predicts that when the IF exceeds the ~100-MHz bandwidth of the mixer block, the impedance of the mixer at the IF will no longer equal the dc dynamic resistance R_d of the pumped I-V curve. No reflection measurements were made at the IFs of 100 or 300 MHz and thus only coupled mixer gain G_c was determined. Accurate mixer noise measurements were not possible with the low IF system due to the lack of cryogenically coolable components at these frequencies.

The apparatus contained a superconducting coil placed around the mixer block which allowed the dc Josephson supercurrent to be easily suppressed. The LHe bath temperature T_b in all of the experiments was < 1.5 K unless otherwise noted.

For each type of junction, mixer performance was measured at bias voltages corresponding approximately to the center or the edge of a photon-assisted tunneling step in the I-V curve. Photon steps were numbered beginning with $n = 1$ for the first step below V_G and n increases as V_0 decreases.

V. RESULTS

A. Mixing with a 1.5-GHz IF

We have made a systematic, quantitative investigation of the effects of I-V curve sharpness and subgap current on mixer performance. The results of mixer experiments with a 1.5-GHz IF for several tunnel junctions are summarized in Table II and discussed below. All measurements were single sideband with a sideband ratio > 18 dB for the Ta junctions, > 20 dB for the Nb junction, and > 23 dB for the Pb-alloy junction.

1. Junction Ta-2: Gain and noise versus photon step and versus subgap current

The mixing properties of the tantalum junction Ta-2 were systematically measured at four bias voltages corresponding to photon steps $n = 1$, 2, and 4 and to a point midway between steps 3 and 4. Figure 1 shows the dc I-V curve

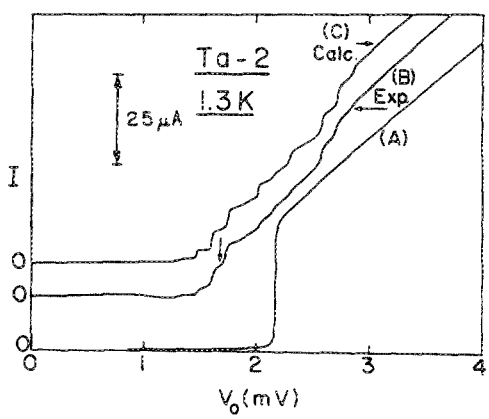

FIG. 1. (A) dc I-V curve without local oscillator (LO) power for the Ta junction Ta-2. (B) Experimental pumped dc I-V curve obtained with the rf tuning and LO power adjusted for the largest coupled gain on photon step $n = 4$. The arrow at 1.65 mV marks the bias voltage for the step $n = 4$ at which best mixer performance was measured. The mixing results are summarized in Table II. (C) Calculated pumped I-V curve with the choice of imbedding impedance $Z_{LO} = 0$ Ω which gives a good fit to the experimental curve (B).

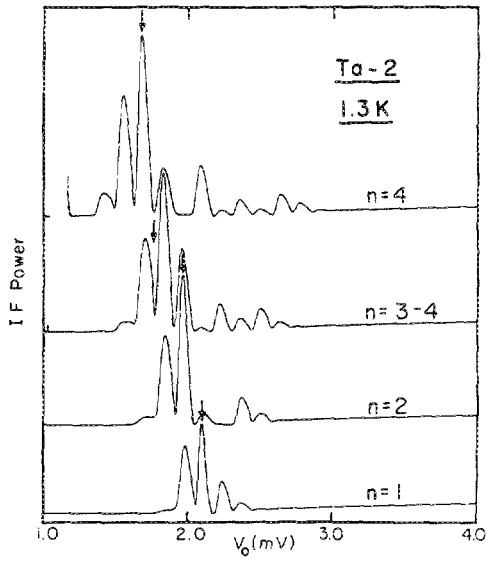

FIG. 2. The IF output power of the mixer vs dc bias voltage with the mixer optimized for largest G_c on the indicated photon step: $n = 1$, 2, 3–4, 4 (3–4 refers to a bias point between steps $n = 3$ and $n = 4$) for junction Ta-2. The zero power levels (not shown) were offset for clarity. The arrows mark the bias voltages at which mixer performance was measured. The best mixer performance was obtained on photon step $n = 4$. The pumped I-V curve corresponding to $n = 4$ is shown in Fig. 1.

for this Ta junction. Curve (A) is without LO power applied, and curve (B) is pumped with LO power which produced best gain on photon step $n = 4$. The photon-assisted tunneling steps are clearly seen in this curve. Figure 2 shows the mixer IF output power with the coupled mixer gain optimized on different photon steps. The expected quantum structure on the scale of $\hbar\omega/e$ is clearly visible in these curves.

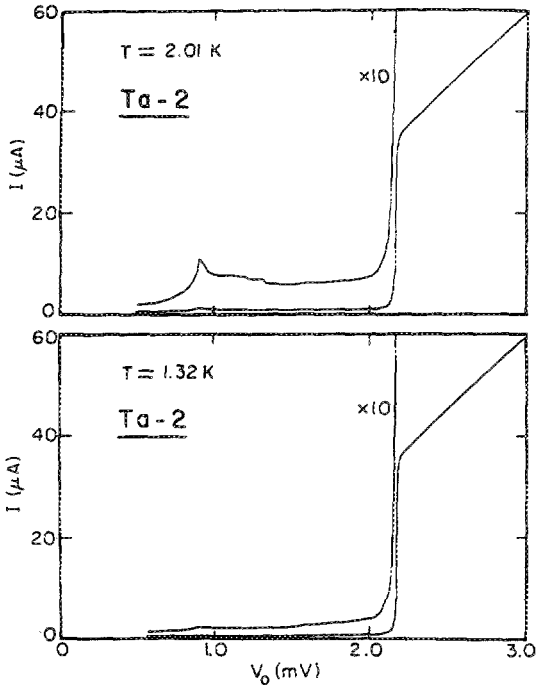

FIG. 3. dc I-V curves for the junction Ta-2 at two different bath temperatures illustrating the increase in subgap current with temperature. There is relatively little change in the sharpness of the current rise at the sum gap.

As seen from Table II, the available gain, G_A, increased significantly with photon step n. On step $n = 4$, G_A increased by a factor of almost 3 over the value on step $n = 1$. T_M decreased with n although the variation was small. The total change was about 1.5 K.

Junction Ta-2 was also measured at an elevated bath temperature. Since the dominant change with temperature was an increase in subgap current, I_{SG}, this provided an excellent opportunity to test the effect of I_{SG} on mixer and receiver performance. Figure 3 shows the dc I-V curve for this junction at $T_b = 1.3$ and 2.0 K. As seen from this figure and the data in Table 1, the width of the current rise at V_G increased by only a factor ~ 1.5, to 31 μV which is still significantly less than $\hbar\omega/e = 150$ μV. The subgap current increased by a factor of 2. This large increase is due, at least in part, to the comparatively low transition temperature, ~ 4.4 K, of the Ta base electrode, which results in a significant increase in thermally excited quasiparticles at 2 K as compared with 1.3 K.

The effects of this change on mixer properties are shown in Table II. The gain, G_A, remained unchanged at 0.41 dB, T_M increased by only 9%, and T_R decreased slightly with bath temperature. Thus, both mixer and receiver performance were only slightly affected by a 100% increase in subgap current I_{SG}. It is shown in Sec. VI that this weak dependence of T_M on I_{SG} is consistent with theory.

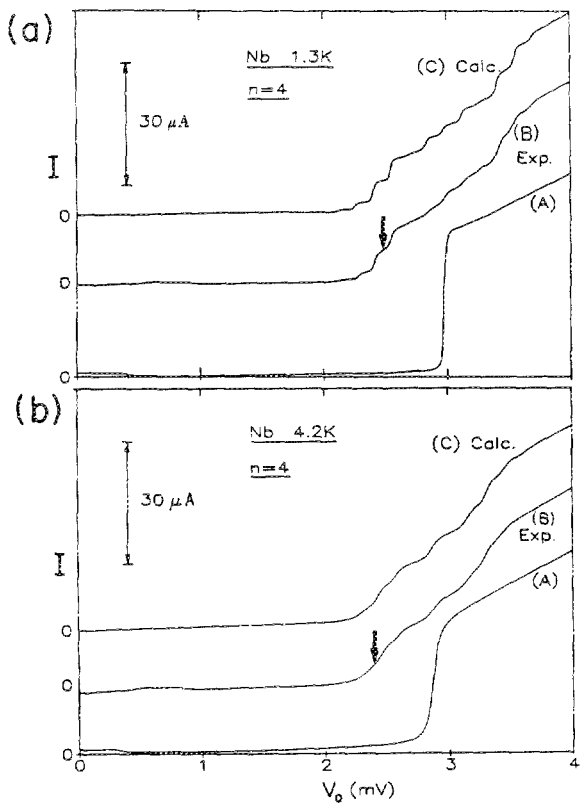

FIG. 4. (a) $T_b = 1.3$ K and (b) $T_b = 4.2$ K; (A) dc I-V curves for the Nb junction. (B) Experimental pumped I-V curve with the rf tuning and LO power adjusted for largest coupled gain on photon step $n = 4$. The vertical arrow marks the bias voltage at which mixer performance was measured. (C) Calculated pumped I-V curve with the choice of imbedding impedance $Z_{LO} = 0$ Ω which gives a good fit to the experimental curve (B).

The SSB receiver noise temperature for our test system was also measured for this junction and the results are listed in Table II. T_R was generally less than 54 K and was dominated by the IF system noise temperature of ~ 15 K. Thus, as the coupled mixer gain increased, T_R decreased. The lowest T_R was 24 K for a tuning which maximized the coupled mixer gain, though the available gain of -0.81 dB in this case was less than the maximum observed. This is the lowest noise measured for such a heterodyne system.

2. Junction Ta-1: Lowest noise mixer

Tantalum junction Ta-1 gave the lowest mixer noise temperature measured to date with $T_M = 3 \pm 1$ K. This is less than twice the quantum limit of $T_Q = 1.7$ K at our operating frequency. The available gain, $G_A = -4.7$ dB, was less than that of the other Ta junctions and may have been due in part to the use of a pure Pb counterelectrode which produced a more rounded I-V curve (see values of ΔV_G in Table I). This rounding is likely due to anisotropic gap values in the polycrystalline grains.

3. Nb junction at 1.3 and 4.2 K: Effect of I-V curve sharpness

The Nb junction was measured at two different bath temperatures in order to observe the effects of the I-V curve quality on mixer performance as discussed in the introduction. Figure 4 shows the dc I-V curves with and without LO power applied at 1.3 and 4.2 K. The changes in the unpumped curve are readily compared in this figure. Also, as seen from Table I, ΔV_G increased by the large factor of 7 as T_b increased to 4.2 K. Thus, ΔV_G increased from less than $\hbar\omega/e$ to about $1.7\hbar\omega/e$. This broadened current rise is due in part to the reduced quasiparticle lifetime in the PbBi counterelectrode at the higher bath temperature.[27]

The results in Table II show that as the bath temperature was increased, G_A decreased by a factor of 2, T_M increased by a factor 1.6, and T_R increased also by a factor of about 2. It is clear that as T_b increases and the quasiparticle nonlinearity changes from $\Delta V_G < \hbar\omega/e$ to $\Delta V_G > \hbar\omega/e$, the performance of the mixer is significantly reduced. However, the computer modeling discussed in Sec. VI predicts an even larger change in performance.

4. Pb-alloy junction at 1.3 K: Gain and noise versus photon step and magnetic field

The mixing properties of the Pb-alloy junction were systematically measured at four bias voltages corresponding to photon steps $n = 4$, 6, and 8 and to a point midway between steps 7 and 8. Figure 5 shows the dc I-V curves with and without LO power applied. Due to the large value of $\Delta V_G = 330\,\mu$V as compared with $\hbar\omega/e = 150\,\mu$V at 36 GHz for this junction, photon-assisted tunneling steps are not readily discernible.

As seen from Table II, the available gain increased with photon step n but the dependence was not strong. The gain

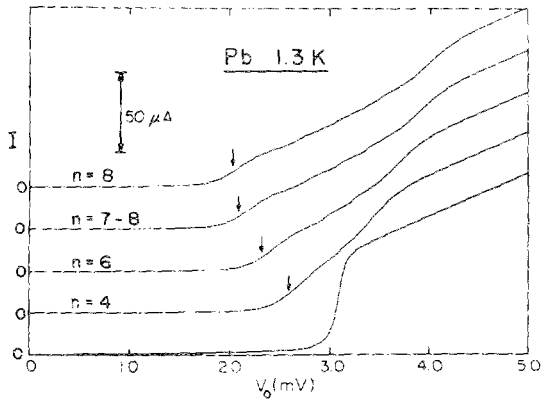

FIG. 5. Experimental pumped dc I-V curves for the Pb-alloy junction. The lowest curve was obtained without LO power. The arrows show the bias voltages where the mixer rf tuning and LO power were adjusted for the largest coupled gain on the indicated photon step: $n = 4$, 6, 7–8, 8 (7–8 refers to a bias point between steps $n = 7$ and $n = 8$). The mixing results are listed in Table II.

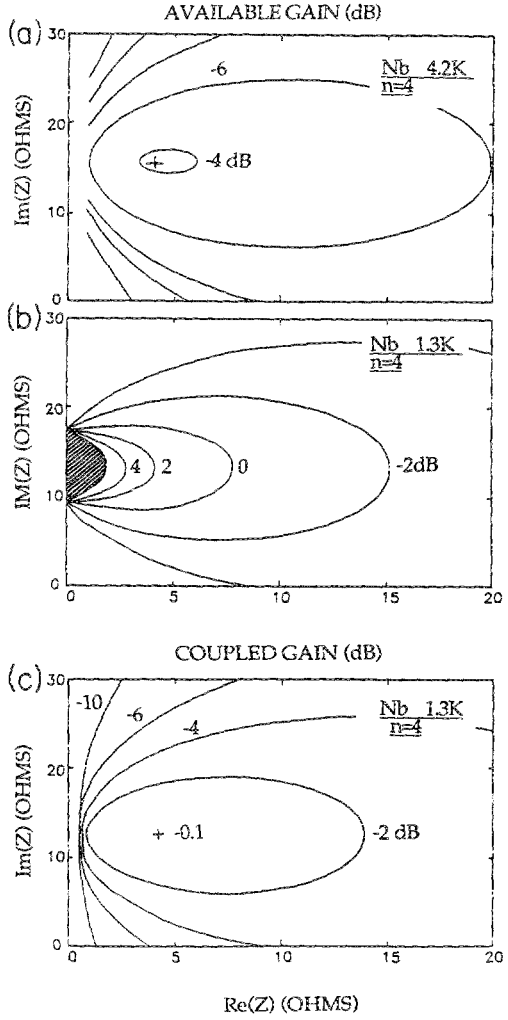

FIG. 6. (a) Calculated contour plot of available mixer gain G_A in dB vs Z_S for the Nb junction at 4.2 K on photon step $n = 4$ ($V_{LO} = 0.58$ mV and the image impedance $Z_I \cong 0\ \Omega$). (b) Contour plot of G_A for the Nb junction at 1.3 K on the photon step $n = 4$ ($V_{LO} = 0.68$ mV and $Z_I \cong 0\ \Omega$). The shaded region has infinite G_A. (c) Contour plot of coupled gain G_c for the same conditions as plot (b) with an IF load impedance of 50 Ω. The experimental value was $G_c = -2.6$ dB.

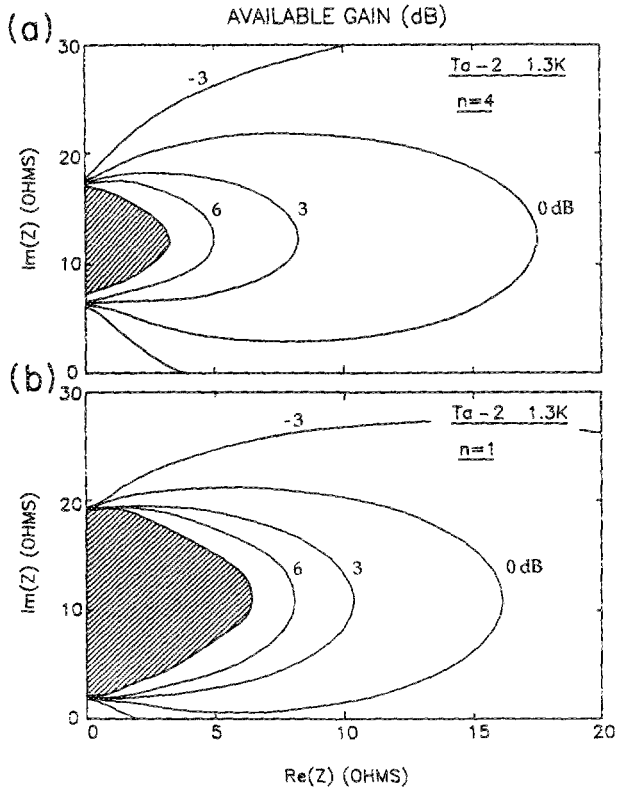

FIG. 7. (a) Calculated contour plot of the available mixer gain G_A in dB vs Z_S for junction Ta-2 on photon step $n = 4$ ($V_{LO} = 0.70$ mV and the image impedance $Z_I = 0\ \Omega$). The shaded region has infinite G_A. (b) Contour plot of G_A vs Z_S for Ta-2 on photon step $n = 1$ ($V_{LO} = 0.20$ mV and $Z_I = 0\ \Omega$). Note the increased size of the infinite gain region as compared with the $n = 4$ plot.

G_A on step $n = 8$ increased by only a factor 1.3 over the value on step $n = 4$. The noise T_M decreased with n, but as with the tantalum junction Ta-2, the variation was only a few degrees. The SSB receiver noise temperature ranged from 58 K on step $n = 4$ to 43 K on step $n = 8$. As with the other junctions discussed so far, T_R was dominated by the IF system noise due to the low mixer gain. The large error limits on these values of T_R are the result of using Eq. (10) to estimate the receiver noise as discussed in Sec. IV.

Gain and noise measurements with and without an applied external magnetic field were also made on the Pb junction optimized on step $n = 8$. The field from a superconducting coil was adjusted to minimize the observed IF noise level at bias voltages near step $n = 8$ and below. This resulted in a complete suppression of the dc Josephson supercurrent. No changes in the mixer tuning were made between measurements with and without a field. The mixer gain was similar in both cases: $G_A = -4.4 \pm 0.2$ dB without a magnetic field and $G_A = -4.5 \pm 0.2$ dB with a field. The effect on mixer noise was also small since $T_M = 6.8 \pm 0.6$ K without a field and $T_M = 6.5 \pm 0.6$ K with a field.

B. Mixing with a low IF

The experimental results for the Ta junctions, using a 1.5-GHz IF, did not show the large gain that can be achieved with such high quality tunnel junctions.[1] By adjusting the backshort and screw tuner, values of the LO embedding impedance could be found that produced regions of negative dynamic resistance R_d on as many as five photon steps.[6] For a low enough IF that the mixer IF output impedance is equal to R_d, Tucker has shown[7] that negative R_d leads to infinite available mixer gain. For such a low IF, the embedding impedances at the signal and image frequencies are the same as the LO impedance, which affects R_d. However, the rf bandwidth of our mixer block was narrow compared with the 1.5-GHz IF and provided different embedding impedances at the signal and LO frequencies. Thus, we found that the signal was poorly matched when the rf coupling was adjusted to provide the proper LO impedance for negative resistance steps. Low values of gain, $G_A \ll -10$ dB, were observed under these conditions.

To explore the effects of rf bandwidth, measurements of the best coupled gain G_c were also made with IFs of 25, 100, and 300 MHz using Ta junctions, Ta-3 and Ta-4. The results are listed in Table III. For each measurement, the coupled gain of the upper sideband was optimized. The available gain G_A was calculated for the 25-MHz measurements using Eqs. (2) and (3) and assuming that R_d was equal to the mixer output impedance as discussed in Sec. III.

Junction Ta-3 produced the largest measured mixer gain, $G_A = 6.7$ dB and $G_c = 2.0$ dB, with an IF of 25 MHz on photon step $n = 1$. The sideband ratio was 0.8 dB. The largest G_c occurred when R_d on the first photon step approached 500 Ω. Larger or negative values of R_d produced smaller coupled gains. The fact that the coupled gain remained finite as R_d and the impedance mismatch became infinite ($|\rho|^2 = 1$) indicates that infinite gain was available for a matched IF load. This observation is consistent with previous experiments.[1,28]

For junction Ta-4, a systematic study of the variation of mixer gain with IF was made and the results are summarized in Table III. The highest coupled gain, $G_c = 0.8$ dB, was found on photon step $n = 1$ with an IF of 25 MHz. The available gain was $G_A = 1.4$ dB with $R_d = 107\ \Omega$. Other photon steps always gave lower values of G_c with a 25-MHz IF. The sideband ratio was only 0.1 dB, indicating nearly complete double-sideband operation. After optimizing the rf tuning for the highest G_c with a 25-MHz IF, the IF was varied by changing the signal frequency with a fixed LO frequency. The 3-dB bandwidth obtained in this way was ~100 MHz.

TABLE III. Summary of mixer results with low intermediate frequencies (IF). The available gain G_A for the 25-MHz measurements was estimated using Eqs. (2) and (3) with $Z_{IF} = R_d$ as discussed in Sec. III. The coupled gain G_c of the upper sideband was optimized in each case. The symbol ** means not measured.

Junction	IF (MHz)	Photon step n	G_c (dB)	G_A (dB)	Sideband ratio (dB)
Ta-3	25	1	2.0	6.7	0.8
Ta-4	25	1	0.8	1.4	0.1
	100	3	−1.9	**	6.6
	300	4	−2.8	**	11.6

When optimized with a 100-MHz IF, this mixer gave a coupled gain, $G_c = -1.9$ dB, which was obtained on photon step $n = 3$. The sideband ratio increased to 6.6 dB and the 3-dB bandwidth increased to ~ 200 MHz.

Finally, with a 300-MHz IF, junction Ta-4 showed its largest coupled gain $G_c = -2.8$ dB on photon step $n = 4$. The 3-dB bandwidth remained fixed at ~ 200 MHz while the sideband ratio increased to about 12 dB. Almost exactly the same results were obtained when G_c of the lower sideband was optimized.

C. Discussion of results

In general, the "sharp" Ta junctions gave the highest mixer gains and lowest mixer noise. The Nb and Pb-alloy junctions gave poorer performance with their more "rounded" I-V curves. A comparison of the mixer results in Table II with the junction properties listed in Table I shows some general trends. The junctions with the lowest values of ΔV_G, and the lowest subgap current gave the best overall performance: large gain and low noise. The measurements on the Nb and Ta junctions at increased T_b also show that at our frequency of 36 GHz the gap sharpness has a stronger influence on mixer performance than subgap current. An increase in the subgap current by a factor of 2 caused no significant degradation in mixer or receiver performance when using sharp junctions ($\Delta V_G < \hbar\omega/e$). At frequencies of ~ 100 GHz and higher, however, gap sharpness will be less important and subgap current may be the more important factor since it will affect mixer noise. Mixer gain greater than unity[4,11] and excellent receiver[2,11] performance near 90 GHz have been reported with "rounded" Pb-alloy junctions similar to the type studied here.

The interaction of Josephson pair currents with quasiparticle currents in an SIS mixer has been theoretically investigated by a few authors.[29,30] The fact that a magnetic field of $\sim 10^{-2}$ T had little effect on mixer gain or noise suggests that Josephson currents are not important for our measurements in any case. For our typical bias voltages, the ac Josephson currents have a frequency of 10^2–10^3 GHz and should be strongly shunted by the junction capacitance. Our measurements are the most sensitive test to date for the influence of Josephson effects on mixer noise.

Measurements with low intermediate frequencies showed that gain increased as both the IF and the sideband ratio decreased. The highest gain was observed on photon step $n = 1$ with a sideband ratio of near unity. This agrees with the prediction of the Tucker theory that best performance should occur on the first step for a DSB mixer. Smith and Richards,[31] D'Addario,[3] and Feldman and Face[32] have pointed out that a double-sideband SIS mixer should yield higher gain than a single-sideband mixer with a shorted image termination. It was also found that as the IF increased, the optimum gain occurred on photon steps with larger n. This result is contrary to theoretical calculations based on a DSB model.[5] We have performed computer simulations of our SSB mixer results and found that for proper choice of image termination that best mixer performance is indeed predicted for $n > 1$. This result is discussed in more detail in Sec. VI.

VI. THEORETICAL MODELING

We have calculated mixer performance for the 1.5-GHz IF experiments using the Tucker theory[7] in the three-port approximation.[5] Our calculations do not make the low IF approximation as is done in most other work (see, for example, Ref. 5) (this low IF approximation has been tested in a few cases, however, and found to be quite accurate[33]). The input data required by the theory are the dc I-V curve, the bias voltage, the LO voltage amplitude V_{LO}, the rf embedding impedances Z_S and Z_I at the signal and image frequencies, respectively, and the IF load impedance Z_L. The junction capacitance C_J, which is included in the rf source impedance in the theory, is also required.

The LO voltage amplitude V_{LO} was determined by fitting the pumped I-V curve as discussed in Sec. VI A below. The IF load impedance Z_L was assumed either to be matched to the mixer IF output impedance, thus yielding available gain G_A, or set to 50 or 100 Ω to investigate the effects of an IF impedance mismatch.

We attempted to determine the rf embedding impedances Z_S and Z_I by using a 3–5-GHz scale model of our rf mixer block.[25] The values of Z_S and Z_I from the scale model do not include the junction capacitance C_J. For all of the junctions measured, we found that the optimum rf tuning was a very sensitive function of the backshort position. This sensitivity to backshort position resulted in large uncertainties in our determination of Z_S from the scale model. For the mixing experiments with the Pb-alloy junction, the scale model predicted a range of Z_S in the inductive half of the Smith chart for which reasonable agreement between theory and experiment was obtained. This was not the case for the Nb and Ta junctions, however. For these junctions, the rf embedding impedances were treated as free parameters. As the calculations presented below (in Secs. VI B and VI C) show, the optimum mixer performance was obtained for values of Z_S in the inductive half of the Smith chart.

All of the noise calculations include the zero-point fluctuation noise ($P_N = \hbar\omega B/2$) of the image and signal impedances as discussed in Sec. III C. Since all of the model calculations were performed for single-sideband mixers (with poor image frequency coupling), the image termination noise was not significant.

A. Pumped I-V curves

In order to model the pumped dc I-V curve, the magnitude of the LO voltage source, V_{LO}, and the complex embedding impedance Z_{LO} must be determined. We relied on a visual comparison of the experimental pumped I-V curve to a series of theoretical pumped curves in order to determine the best values for V_{LO} and Z_{LO}. This approach has been used successfully by other authors.[34] Z_{LO} was treated as a free parameter and V_{LO} was chosen to force the pumped dc current to match the experimental value at the bias voltage for which the best mixer performance was observed. The value of V_{LO} determined in this way was used in the calculation of mixer gain and noise.

We found that small values of the LO embedding impedance, $|Z_{LO}| < 5$ Ω, yielded a good fit to all of the pumped

I-V curves (Pb-alloy, Nb, and Ta) for experiments with a 1.5-GHz IF. All of the calculations for the pumped I-V curves have been performed with $C_J = 300$ fF. Figure 1 compares the experimental and calculated pumped I-V curves for junction Ta-2 at 1.3 K. Figure 4 shows the experimental and calculated curves for the Nb junction at 4.2 and 1.3 K. The quality of the fit is easily seen by comparing the measured and calculated curves and is comparable to that found by other authors.[34]

The small value of Z_{LO} discussed above indicates a large impedance mismatch between the junction and the mixer block at the LO frequency. This mismatch is a result of the narrow bandwidth of our mixer block. The image frequency was also strongly mismatched as indicated by the large sideband ratios discussed in Sec. V.

B. Pb-alloy junction: Weak quantum effects

For the Pb-alloy junction, quantum effects were weak since $\Delta V_G = 330\,\mu$V was larger than $\hbar\omega/e$ ($150\,\mu$V). In this regime, the theoretical calculations, which model mixer performance on the photon steps previously discussed in Sec. V, show the best agreement with the experiment.

Available mixer gain and noise temperature were calculated versus the source impedance Z_S for the ranges $0 \leqslant \mathrm{Im}|Z_S| \leqslant 30\ \Omega$ and $0 \leqslant \mathrm{Re}|Z_S| \leqslant 20\ \Omega$. Contour plots similar in form to those in Figs. 6(a) and 8, for Nb and Ta junctions discussed in Secs. VI C and D, respectively, below, were obtained. The junction capacitance was adjusted to 350 fF to yield a maximum in the gain on photon step $n = 8$ approximately centered in the given range of Z_S and was then held fixed for calculating the mixer performance on the other photon steps (this value of C_J is lower than estimated from Ref. 16 but was required to obtain reasonable agreement with the experiments; it also reduces the value of $\omega_S R_N C_J$ in Table I to about 3). The image impedance was chosen to be $Z_I = 0.01 + j0.01\ \Omega$, essentially a short circuit. This gave the closest agreement between theory and experiment. Image terminations other than a short circuit were investigated, but were usually found to predict largest gain on photon steps with smaller n, which is in contrast to the experimental results. In general, we found that the predicted gain versus bias voltage is strongly dependent on the choice of image termination. In contrast, most other published calculations assume equal signal and image terminations (i.e., a DSB mixer) and thus predict best performance on the first photon step.

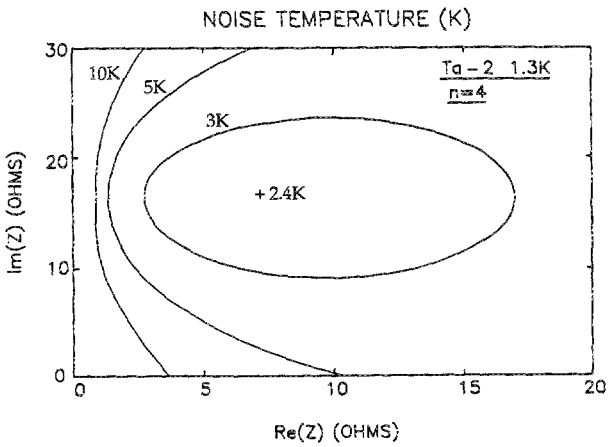

FIG. 8. Calculated contour plot of mixer noise temperature T_M vs Z_S for junction Ta-2 on photon step $n = 4$ [$V_{LO} = 0.70$ mV and the image impedance $Z_I = 0\ \Omega$; these are the same conditions as in Fig. 7(a) for mixer gain]. T_M approaches the quantum limit $T_Q = \hbar\omega/k_B = 1.7$ K at 33 GHz. The experimental value was $T_M = 3.9 \pm 0.4$ K.

The theoretical calculations for each photon step are summarized in Table II and compared to experiment. It can be seen that with the exception of step $n = 8$ the theory overestimates the gain. This result is expected from a three-port model if significant harmonic conversion is present. This issue is discussed in more detail in Sec. VI F. The theoretical values lie just outside the experimental error limits on steps $n = 6$ and 7–8, although the discrepancy is not severe. The agreement with experiment is excellent on the other steps.

The theory significantly underestimates the mixer noise temperatures and the predicted values are clearly outside the experimental error limits. This result holds as well for the other junctions (Ta and Nb) as seen in Table II. We find the ratio of the experimental to the theoretical noise temperature in almost every case studied is close to the value 2 (except for the Nb junction measured at a bath temperature of 1.3 K where this ratio drops to about 1.5). Possible explanations for this discrepancy are discussed in Sec. VI F.

C. Nb junction: Weak and strong quantum effects

As discussed in the introduction, this junction provided a good test of the theory when quantum effects were weak or strong, due to the temperature dependence of the width ΔV_G of the current rise. At 4.2 K, ΔV_G exceeded the characteristic photon voltage $\hbar\omega/e$. However, when cooled to 1.3 K, the I-V curve became considerably sharper, $\Delta V_G < \hbar\omega/e$, and had lower subgap current. It then showed stronger quantum effects such as the sharper photon steps seen in Fig. 4. Figure 6(a) shows contours of constant available gain versus the real and imaginary parts of Z_S for the junction at 4.2 K biased on photon step $n = 4$. The range of $\mathrm{Im}(Z_S)$ was chosen to include values of inductive reactance which would resonate with the junction capacitance. The image impedance was chosen to be almost a short circuit: $Z_I = 0.01 + j0.01\ \Omega$. This gave the closest agreement between theory and experiment. Other image terminations predicted largest gain on photon steps closer to the gap. For a model in which the image is open circuited (except for the capacitive susceptance of the junction in parallel), the calculations predicted a large coupled gain (into $Z_L = 50\ \Omega$) of $+8$ dB on the first photon step and a much smaller gain, -2 dB, on step $n = 4$. This clearly contrasts with the experimental results.

As seen from Table II, the available gain predicted by the theory is significantly larger than the measured value and is well outside the error limits. However, this predicted value is finite which is not the case when the junction is modeled at 1.3 K as discussed below.

Figure 6(b) shows a computed contour plot of available gain for the Nb junction at 1.3 K. The most striking feature

of this plot is the appearance of regions of $G_A > 0$ dB and infinite available gain (shaded region). These predictions disagree strongly with the experimental results listed in Table II where $G_A < 0$ dB. The fact that we did not observe infinite G_A or even $G_A > 0$ dB is surprising since the mixer block could provide the necessary range of Z_S. One possibility is that by optimizing the mixer for best coupled gain we have missed regions of large available gain. This is not usually a problem when the mixer sees the same impedance at the LO, signal, and image frequencies because flat steps or negative resistance appear on the pumped I-V curve to indicate large available gain. When the LO impedance is significantly different from the signal impedance, as in our case, the correlation of flat or negative resistance steps with large gain no longer exists. In fact, as pointed out in Sec. V, the tuning conditions that produced flat steps on the pumped I-V curve of a Ta junction produced very poor mixer performance. In order to check for the possibility that maximizing the coupled gain may not locate regions of large available gain, we have calculated the coupled gain for the Nb junction with a 50-Ω IF load impedance and a short-circuit image at both 4.2 and 1.3 K. At 4.2 K, the result is essentially identical to that shown in Fig. 6(a) and hence the coupled and available gain are maximum for the same Z_S. As shown in Fig. 6(c), however, the coupled gain at 1.3 K is maximum for $\mathrm{Re}(Z_S) \sim 4\ \Omega$, which is outside the region of infinite available gain as seen in Fig. 6(b). This result suggests that it is possible to miss regions of very large G_A when optimizing the coupled gain, but it does not explain our discrepancy since we should have measured at least $G_A > 0$ dB. With $Z_L = 50\ \Omega$, we calculated a coupled gain $G_c = -0.1$ dB, which is at least finite, but exceeds the experimental value by a factor of about 2.

D. Tantalum junction Ta-2: Strong quantum effects

Tantalum junction Ta-2 had the sharpest I-V curve and lowest subgap current. ΔV_G was as low as 22 μV which is a factor of about 7 smaller than $\hbar\omega/e$. This junction provided a good test of the theory in the limit where quantum effects are strong.

Mixer performance was modeled on photon steps $n = 1$, 2, 4, and between steps 3 and 4. Figure 7 shows contour plots of available gain versus Z_S for steps $n = 1$ and 4. Figure 8 shows calculated noise temperature contours versus Z_S for step $n = 4$. The imaginary part of Z_S approximately tunes out the junction capacitance for best available gain. The image impedance was chosen to be a short circuit for each calculation.

Table II summarizes the calculated results and compares them with measured values. The theory clearly predicts infinite available gain for each photon step except $n = 3$–4, where the theory overestimates the gain by only 1 dB. In addition, as seen from Fig. 7 the size of the infinite gain region increases for photon steps with smaller n. This result was also true for the Nb junction. This result is in sharp contrast to the experiments which showed available gain decreasing with n.

As with the Nb junctions, we investigated the possibility of missing large available gain by optimizing the coupled gain. However, calculations of the coupled gain for several IF impedances indicated that it is virtually impossible to miss the regions of infinite available gain by maximizing the coupled gain. This implies that we should have measured a large IF mismatch and large available gain for each experimental bias point, which was clearly not the case.

It is also clear, from Table II, that the predicted noise temperatures are significantly below the measured values. In each case, the calculated value is well outside the experimental error limits.

Despite the disagreement in available gain, we calculated the dependence of coupled gain on bias voltage with a fixed 50-Ω IF load for both the Nb and Ta junctions. We found good agreement between theory and experiment for the relative variation of coupled gain versus bias voltage for both junctions. However, the absolute magnitudes were not correctly predicted.

E. Mixer noise versus subgap current

Measurements were also performed on junction Ta-2 at a bath temperature of 2.0 K for which there was a substantial increase in subgap current as discussed in Sec. V. In order to compare the experimental results for the variation of mixer noise due to increased subgap current with the theory, we have modeled the mixer noise for the two bath temperatures: 1.3 and 2.0 K. As with the previous calculations discussed for this junction, the predicted mixer gain was substantially larger than the observed value and the predicted noise was about a factor of 2 smaller than the measured value at a bath temperature of 2.0 K. However, the predicted increase in noise was 0.4 K which is in excellent agreement with the experimentally observed increase of ~0.4 K. Again we find that the theory predicts a relative variation with greater accuracy than the absolute magnitudes.

F. Discussion of modeling results

From the results of computer calculations, we find that the Tucker theory predicts mixer gain with reasonable accuracy when the I-V curve is rounded and quantum effects are weak. However, as the I-V curve becomes sharper and quantum effects become stronger, theory and experiment begin to diverge significantly, as was the case for our Nb and Ta junctions.

The predictions of mixer noise temperatures based on the Tucker quantum shot-noise theory were about a factor of 2 smaller than the measured values in almost every case. There are two possible explanations for this discrepancy. Either the three-port model is incorrect or additional sources of noise were present. We will discuss the latter possibility first. One possible source of additional noise was our klystron local oscillator. A recent estimate[35] for the signal-to-noise ratio in a klystron gives 170 dB in a 1-Hz bandwidth at 1.5 GHz from the operating frequency. This implies a very small added noise at the mixer block of less than 0.01 K for an LO power of 10 nW which is typical for a well-matched junction. However, due to the narrow, ~100 MHz, bandwidth of our mixer block the LO was poorly matched and power levels approaching 1–10 μW at the mixer block were required to properly pump the junctions. Under these condi-

tions, the LO noise might become significant: 1–10 K. Due to the difficulty involved, no attempts were made to measure the signal-to-noise ratio for our Ka band klystron. However, a rough estimate of the LO noise can be made from measurements on array mixers performed by some of the authors[36] in the same apparatus using the same measurement techniques and frequencies discussed in this paper. The array mixers required significantly greater LO power than single junction mixers. If we take as a limiting case that all the noise measured in the array mixers resulted from the LO and assume that this noise contribution scales with the LO power level, then an upper limit for this noise can be estimated from the LO power required for the single junction mixers discussed here. For example, a 25-junction array mixer with $\omega_s R_N C_J = 3.2$ and $G_A = 5.6$ dB (values comparable to those studied here) required an LO power of about 36 μW and gave a mixer noise temperature of 12 K. This would imply a maximum LO noise for the Ta junction experiments of 0.7 K where the maximum LO power was about 2 μW. Other array mixers with different values of $\omega_s R_N C_J$ and G_A gave similar estimates of 0.1–1 K. This example suggests that the LO noise contribution is too small to account for the observed differences with theory, but clearly we cannot completely rule out this source of extra noise.

It is also unlikely that Josephson effects were contributing significant noise. As discussed in Sec. V, the Pb-alloy junction was measured with and without an external magnetic field. The result with the field applied was only 0.3 K lower than without it. This is much less than the observed discrepancy and does not significantly improve the agreement. Estimates of the losses in the waveguide mixer block and the IF matching transformer indicate that noise from these components was negligible. We can find no other sources of noise which would contribute significantly to our experimental results.

The other possible explanation for our discrepancy is that the three-port quantum model is not applicable. The low-noise levels in an SIS mixer depend on a detailed correlation of noise contributions from the fundamental as well as the harmonic frequencies and thus are sensitive to the embedding impedances at these frequencies. The harmonic response is entirely neglected in the three-port model and this might account for the discrepancy we find. Evidence that harmonic effects may be important for some of our mixers is discussed below in connection with the gain calculations.

The best agreement between theory and experiment for mixer gain was found for the Pb-alloy junction. We do not expect a significant contribution from harmonics in this mixer with $\omega_s R_N C_J \sim 3$–6. Other workers [37] have also found good agreement with theory for junctions with similarly rounded I-V curves and $\omega_s R_N C_J = 4$. The junction capacitance is expected to strongly shunt the harmonic frequencies. However, this may not be the case in our Nb and Ta junctions which were substantially more nonlinear than the Pb-alloy junction. Harmonic conversion is expected to make a more significant contribution in these sharp junctions and the effect should be more pronounced near the gap voltage. Shen *et al.*,[38] for example, also found a predicted divergence in mixer gain for small n using a three-port model. They reported preliminary five-port model calculations for which this divergence vanished and finite gain was predicted. Other reported results with sharp I-V curves also showed substantially less gain than predicted by three-port modeling.[1] Additional calculations which include first harmonic effects may help to resolve the discrepancy with mixer gain and may also improve the agreement for the noise temperatures as well. Due to the computational difficulties, we have not attempted this more ambitious project.

In addition, our calculations for the Nb and Ta junctions indicated that an open-circuited, or purely reactive, image termination may be best suited for obtaining large mixer gain. Feldman and Face [32] have recently shown that the range of source conductance which leads to $G_A > 0$ dB is strongly dependent on the choice of image termination. In particular, an open circuit produces the largest range in Z_s and a short-circuited image leads to the smallest range of required Z_s. A similar conclusion has been previously reached by D'Addario.[3]

VII. SUMMARY

We have made a systematic study of the gain and noise in SIS mixers employing Ta based, Nb based, and Pb-alloy based tunnel junctions. These junctions displayed both strong and weak quantum effects at a signal frequency of 33 GHz. In order to make accurate measurements, we have used a novel test apparatus which is accurate enough to allow for the first detailed tests of the theoretical noise predictions. Detailed comparisons of the mixing results with the predictions of the Tucker theory were made.

The Ta junctions which had the sharpest I-V curves, $\Delta V_G \ll \hbar\omega/e$, and the lowest subgap current gave the best performance. The Pb-alloy and Nb junctions with $\Delta V_G > \hbar\omega/e$ and higher subgap current gave poorer performance. In general, as ΔV_G and the subgap current increased, mixer gain decreased and mixer noise increased. However, substantial increases in subgap current with $\Delta V_G \ll \hbar\omega/e$ had little effect on mixer gain or noise. In addition, DSB mixers produced $G_A > 0$ dB while SSB mixers provided $G_A \sim 0$ dB. Theoretical modeling suggested that the SSB mixers had a short-circuited image termination, and that lower gain is expected for shorted image SSB mixers as compared to DSB mixers.

Theoretical predictions with a three-port model overestimated the mixer gain in every case and in most cases the predictions were well outside the limits of experimental error. For junctions with $\Delta V_G > \hbar\omega/e$ and showing weak quantum effects, the theory predicted finite available gain. For junctions with $\Delta V_G < \hbar\omega/e$ and showing strong quantum effects, the theory predicted infinite available gain. According to the theoretical calculations, the range of rf signal impedances for which these divergences occurred increased for mixing on photon steps closer to the sum gap voltage. The theory also predicted noise temperatures that were almost a factor of 2 smaller than the measured values and were well outside the experimental error limits. A five-port mixer model which includes effects due to first harmonic conversion may help to resolve these discrepancies.

We also found that the predicted coupled gain versus bias voltage is strongly dependent on the choice of image termination. In particular, with a short-circuited image termination the theory predicts that the maximum gain will occur on photon steps $n > 1$. This agrees with our experimental observations for SSB mixers. For a DSB mixer, the theory predicts best performance on the first photon step. This also agrees with our results for DSB mixers with a low IF.

Our systematic study of mixer performance should be useful in the design of SIS receivers. Given the complexities of tunnel junction fabrication, it is desirable to know the required energy gap sharpness and subgap current for a particular signal frequency. In addition, since low-noise operation is usually a primary goal for a receiver, our low test system noise temperature of 24 K is encouraging. It suggests that receivers with noise levels approaching the quantum limit can be built.

ACKNOWLEDGMENTS

We are grateful to A. V. Räisänen for assisting with the 25-MHz IF measurements. We are also indebted to T. Lum, J. Welch, and D. Williams of the Radio Astronomy Laboratory, University of California, Berkeley for supplying the GaAs field-effect-transistor IF amplifier and for the use of their network analyzer. We also thank A. D. Smith for initial contributions to the mixer calculation programs. This work was supported by ONR Contract Nos. N00014-80-C-0855 and N00014-85-C-0233, the U.S. Air Force Office of Scientific Research Grant No. 85-0230, and by NSF Grant Nos. ECS8305000 and ECS8604350.

[1]W. R. McGrath, P. L. Richards, A. D. Smith, H. van Kempen, R. A. Batchelor, D. E. Prober, and P. Santhanam, Appl. Phys. Lett. **39**, 655 (1981).
[2]L. Olsson, S. Rudner, E. Kollberg, and C. O. Lindstrom, Int. J. Infrared Millimeter Waves **4**, 847 (1983); S.-K. Pan, M. J. Feldman, A. R. Kerr, and P. Timbie, Appl. Phys. Lett. **43**, 786 (1983); E. C. Sutton, IEEE Trans. Microwave Theory Tech. **MTT-31**, 589 (1983); M. J. Wengler, D. P. Woody, R. E. Miller, and T. G. Phillips, Int. J. Infrared Millimeter Waves **6**, 697 (1985).
[3]L. R. D'Addario, Int. J. Infrared Millimeter Waves **5**, 1419 (1984).
[4]A. V. Räisänen, D. G. Cre'te', P. L. Richards, and F. L. Lloyd, Int. J. Infrared Millimeter Waves **7**, 1835 (1986).
[5]J. R. Tucker and M. J. Feldman, Rev. Mod. Phys. **57**, 1055 (1985).
[6]D. W. Face, D. E. Prober, W. R. McGrath, and P. L. Richards, Appl. Phys. Lett. **48**, 1098 (1986).
[7]J. R. Tucker, IEEE J. Quantum Electron. **QE-15**, 1234 (1979); J. R. Tucker, Appl. Phys. Lett. **36**, 477 (1980).
[8]C. M. Caves, Phys. Rev. D **26**, 1817 (1982).
[9]M. J. Feldman, IEEE Trans. Magn. **MAG-23**, 1054 (1987).
[10]M. J. Wengler and D. P. Woody, IEEE J. Quantum Electron. **QE-23**, 613 (1987).
[11]A. V. Räisänen, D. G. Cre'te', P. L. Richards, and F. L. Lloyd, *Digest of the IEEE Symposium on Microwave Theory Technology, Las Vegas, 1987* (Institute of Electrical and Electronic Engineers, Inc., Piscataway, NJ, 1987), p. 929.
[12]W. R. McGrath, A. V. Räisänen, and P. L. Richards, Int. J. Infrared Millimeter Waves **7**, 543 (1986).
[13]H.-C. W. Huang, S. Basavaiah, C. J. Kircher, E. P. Harris, M. Murakami, S. P. Klepner, and J. H. Griener, IEEE Trans. Electron Devices **ED-27**, 1979 (1980); and IBM J. Res. Dev. **24**, 105 (1980).
[14]D. W. Face and D. E. Prober, J. Appl. Phys. **62**, 3257 (1987).
[15]R. E. Harris, R. C. Dynes, and D. M. Ginsberg, Phys. Rev. B **14**, 993 (1976).
[16]J. H. Magerlein, IEEE Trans. Magn. **MAG-17**, 286 (1981).
[17]R. F. Broom, S. I. Raider, A. Oosenbrug, R. E. Drake, and W. Walter, IEEE Trans. Electron Devices **ED-27**, 1998 (1980).
[18]E. K. Track, A. Worsham, G.-J. Cui, and D. E. Prober, to appear in *Advances in Cryogenic Engineering*, edited by R. P. Reed and A. F. Clark (Plenum, New York, 1988), Vol. 34.
[19]In this case, $|\rho| \geq 1$ and Eq. (2) is no longer valid.
[20]F. R. Arams, *Infrared-to-Millimeter Wavelength Detectors* (Artech, Dedham, MA, 1973).
[21]A. van der Ziel, *Noise in Measurements* (Wiley, New York, 1976), p. 188.
[22]I. A. Devyatov, L. S. Kuzmin, K. K. Likharev, V. V. Migulin, and A. B. Zorin, J. Appl. Phys. **60**, 1808 (1986).
[23]A. B. Zorin, IEEE Trans. Magn. **MAG-21**, 939 (1985).
[24]R. H. Koch, D. J. Van Harlingen, and J. Clarke, Phys. Rev. B **26**, 74 (1982).
[25]A. V. Räisänen, W. R. McGrath, D. G. Cre'te', and P. L. Richards, Int. J. Infrared Millimeter Waves **6**, 1169 (1985).
[26]D. R. Williams, W. Lum, and S. Weinreb, Microwave J. **23**, 70 (1980).
[27]R. C. Dynes, V. Narayanamurti, and J. P. Garno, Phys. Rev. Lett. **41**, 1509 (1978); and S. B. Kaplan, C. C. Chi, D. N. Langenberg, J. J. Chang, S. Jafarey, and D. J. Scalapino, Phys. Rev. Bca **14**, 4854 (1976).
[28]A. R. Kerr, S.-K. Pan, M. J. Feldman, and A. Davidson, Physica B&C **108**, 1369 (1981).
[29]T.-M. Shen, IEEE J. Quantum Electron. **QE-17**, 1151 (1981).
[30]D. G. Jablonski and M. W. Henneberger, J. Appl. Phys. **58**, 3814 (1985).
[31]A. D. Smith and P. L. Richards, J. Appl. Phys. **53**, 3806 (1982).
[32]M. J. Feldman and D. W. Face, Jpn. J. Appl. Phys. **26**, 1633 (1987).
[33]D. W. Face, Ph. D. thesis (Yale University, New Haven, CT, 1987, available from University Microfilms).
[34]T. G. Phillips and G. J. Dolan, Physica **109** and **110B**, 2010 (1982).
[35]G. A. Ediss, N. J. Keen, and P. Zimmerman, IEEE Trans. Microwave Theory Tech. **MTT-30**, 2012 (1982).
[36]W. R. McGrath, A. V. Räisänen, P. L. Richards, R. E. Harris, and F. L. Lloyd, IEEE Trans. Magn. **MAG-21**, 212 (1985).
[37]M. J. Feldman and S. Rudner, *Reviews of Infrared and Millimeter Waves*, edited by K. J. Button (Plenum, New York, 1983), Vol. 1, p. 47.
[38]T.-M. Shen, P. L. Richards, R. E. Harris, and F. L. Lloyd, Appl. Phys. Lett. **36**, 777 (1980).